

Study of an entropy-consistent Navier–Stokes flux

Akmal Nizam Mohammed^a and Farzad Ismail^{b*}

^a*School of Mechanical Engineering, Universiti Sains Malaysia, Nibong Tebal, Pulau Pinang, 14300, Malaysia;* ^b*School of Aerospace Engineering, Universiti Sains Malaysia, Nibong Tebal, Pulau Pinang, 14300, Malaysia*

(Received 20 October 2011; final version received 20 November 2012)

This paper presents a study to achieve discrete entropy consistency using artificial and physical diffusion mechanisms. The study begins with the one-dimensional viscous Burgers equation, specifically looking at the shock results of entropy-conserved fluxes combined with a few choices of artificial and physical viscous diffusions. The approach is then repeated for the Navier–Stokes equations. Overall, it is demonstrated that the artificial viscosity (or entropy) terms are still needed in addition to physical viscosity to achieve entropy consistency in shock predictions, although one of the artificial terms can be dropped for high viscosity or low Reynolds number flow.

Keywords: shock capturing; Navier–Stokes flux; entropy consistency; entropy production; physical viscosity

1. Introduction

In developing shock-capturing schemes, it is usually difficult to strike a balance between accuracy and practicality. As we strive to improve its shock capturing capabilities, we must also maintain simplicity in the scheme to keep it from being too computationally expensive. Currently, one of the challenges in shock capturing methods is to include auxiliary constraints (i.e. entropy and vorticity control) to the primary constraints (i.e. mass, momentum and energy conservation) in the design of the numerical schemes. For instance, the inclusion of discrete entropy conditions in the numerical flux function. To achieve this, a low-cost, entropy-consistent flux function was proposed in Ismail (2006), Roe (unpublished) and Ismail and Roe (2009). This scheme has been compared to other schemes and was shown to eliminate one-dimensional shock instabilities in Kitamura *et al.* (2009).

The said flux function was constructed from three main ideas that are manifested in the form of three distinct components: entropy conservation, entropy stability and entropy production. Entropy conservation ensures that entropy is neither created nor destroyed, and this is true for smooth flows (Tadmor 1987, Lefloch *et al.* 2002, Roe unpublished). If shocks are present, it is expected that entropy will be generated across this discontinuity. The question remains if entropy is produced with the correct sign and magnitude. Entropy stability ensures that the entropy change within the system is of the correct sign (Barth 1999). The scheme is then said to be entropy consistent if it generates entropy

with the correct sign and magnitude across any discontinuity such as shock or contact discontinuities.

The flux function of Ismail and Roe (2009) was designed to be entropy-stable for shocks (and contact discontinuities) of any strength, but its derivation to achieve entropy consistency was based on weak shocks. For strong shocks, the flux function required some adjustments based on empirical observations, and although the entropy-consistent flux showed good performance on a variety of shock strengths, the whole principle of entropy production was based on inviscid formulation. In this paper, we explore the effects of physical viscosity as a part of the entropy production term similar to the work of Tadmor and Zhong (2006a, b) and Fjordholm *et al.* (2008), but unlike the work we are presenting herein, previous work only worked on one viscosity value. Hopefully, our approach would provide a more complete picture in terms of generating entropy through physical viscosity, which in turn could bring the solution closer to precisely satisfying the second law of thermodynamics.

The idea of incorporating the physical viscosity is first investigated on the viscous Burgers equation where the focus will be on shock predictions. Later, the approach is expanded and applied to the Navier–Stokes equations but without heat transfer, since this is a preliminary study. The schemes of Roe, Tadmor–Zhong (TZV), Entropy Stable with added viscosity (ESV) and Entropy Consistent with added viscosity (EC2V) are tested on steady and unsteady shock problems in one dimension.

*Corresponding author. Email: aefarzad@eng.usm.my

It must be emphasised that it is not easy to analytically relate entropy production to shock quality since most conservation laws only exhibit entropy as a decreasing function without actually having known the precise entropy reduction. Thus, achieving entropy consistency in this paper will mostly be based on numerical experiments. Our objective here is to merely find an ‘acceptable’ viscous shock profile for both the Burgers and Navier–Stokes equations.

2. Burgers’ equation as the basic model

The simplicity of Burgers’ equation makes it ideal as the base model for the viscosity added entropy-consistent flux.

2.1. Entropy conservation, stability and consistency

The entropy-consistent flux function was derived based on the inviscid Burgers equation:

$$\frac{\partial u}{\partial t} + \frac{\partial(\frac{u^2}{2})}{\partial x} = v \frac{\partial^2 u}{\partial x^2}, \quad (1)$$

where $v = 0$. Physical laws require that entropy is always increasing (or decreasing, depending on the point of reference) in a system undergoing a thermodynamic process. Thus, the notion can be expressed in mathematical terms as a decreasing function:

$$\frac{\partial U}{\partial t} + \frac{\partial F}{\partial x} \leq 0, \quad (2)$$

where $U = u^2$, $v = \frac{\partial U}{\partial u}$ and $F = \frac{2}{3}u^3$. Entropy conservation requires that equality is achieved in Equation (2), thus a numerical method that conserves entropy must discretely satisfy equality in Equation (2) such as in Tadmor (1987) and Roe (unpublished). Entropy stability implies that a numerical method discretely satisfies the inequality, as in Barth (1999). The choice of $U = u^2$ reflects the use of numerical entropy instead of its physical counterpart ($S = -u^2$) in calculations involving the Burgers’ equation model. This is to ensure that, whilst the localised entropy may drop due to the change in velocity, its value will always be bounded by zero, and thus the inequality of Equation (2) is enforced without fail. A more detailed discussion on numerical and physical entropy can be found in Hughes *et al.* (1986) and Ismail and Roe (2009). Entropy consistency means that a numerical method produces entropy with the correct sign and magnitude, as in Ismail and Roe (2009). The following discussion briefly presents an entropy-consistent flux function for the Burgers equation.

The inviscid part of Equation (1) is discretised using a semi-discrete finite volume method at cell j with a uniform size of Δx such that

$$\left(\frac{\partial u}{\partial t}\right)_j \Delta x = -(f_{j+\frac{1}{2}} - f_{j-\frac{1}{2}}), \quad (3)$$

where $f_{j\pm\frac{1}{2}} = f^*$ are the fluxes to be evaluated at the respective interfaces. An entropy-consistent flux function would be

$$f^* = f_c - f_s - f_p, \quad (4a)$$

$$f_c = \frac{1}{6}(u_L^2 + u_R u_L + u_R^2), \quad (4b)$$

$$f_s = \frac{1}{4}|u_L + u_R|[u], \quad (4c)$$

$$f_p = \frac{[u][u]}{12}, \quad (4d)$$

where $[\cdot]$ is the difference function, which in this instance $[u] = u_R - u_L$. Equation (4) denotes the flux interface $*$ which is shared by two adjacent cell values denoted by the subscripts L and R representing the left and right cells, respectively. The term f_c represents the entropy-conserved flux (Tadmor 1987, Roe unpublished). Coupling f_c with f_s represents an entropy stable flux of as in Tadmor (2002) and the references therein. The third term f_p represents the production term. Recall that Equation (4a) is also known as the original Roe-flux from Roe (1981) with an entropy fix by Harten and Hyman (1983).

2.2. Entropy generation via added physical viscosity

For the viscous part of Equation (1), a central differencing approach is used. We call this as the added viscosity term. The idea and mechanism of how physical viscosity generates entropy was previously developed in Tadmor (2004). Alternatively, using the approach and the notations developed in Ismail and Roe (2009), entropy generation at each flux interface is defined by the difference of entropy produced by any flux and the entropy produced by an entropy-conserved flux. Therefore, the added physical viscosity and the numerical viscosity terms will generate entropy in the form of:

$$\begin{aligned} \dot{U} &= -\frac{1}{2}(|\bar{a}| + \alpha[a])[u][v] - \frac{v}{\Delta x}[u][v] \\ &= -\frac{1}{2}(|\bar{a}| + \alpha[a])\frac{du}{dv}[v]^2 - \frac{v}{(2\Delta x)}[v]^2, \end{aligned} \quad (5)$$

implying that the discrete physical viscosity term produces a decreasing entropy generation. In Equation

(5), the term $\frac{1}{2}(|\bar{a}| + \alpha[a])\frac{du}{dv}[v]^2$ represents upwinding that ensures entropy stability as prescribed by Equation (2), and if $\alpha = 1/6$ is chosen, we get the inviscid entropy-consistent flux as given in Equation (4). Here, the variable a is the wave speed for the Burgers' equation and \bar{a} denotes its averaged quantity. The term $\frac{du}{dv}[v^2]$, which is just a different way of reflecting the change of u in $[u][v]$, is used since it is a better representation for extension to systems of equations. As mentioned in the introduction section, it is difficult to determine the exact entropy generation across a shock but here at least we are certain that the discrete physical viscosity is producing entropy with the correct sign. Achieving entropy consistency herein will be based on the entropy produced by both the artificial and physical diffusion. Thus, the entropy-consistent flux with physical viscosity added in its final form can be written as

$$f^* = \frac{1}{6}(u_L^2 + u_R u_L + u_R^2) - \frac{1}{4}|u_L + u_R|(u_R - u_L) - \frac{v}{(\Delta x)}(u_R - u_L). \quad (6)$$

2.3. Time discretisation and second-order extensions

Although there are other time integration methods that can be used, herein a second-order Runge–Kutta time discretisation method was used to solve Equation (1), where:

$$u^{n+1} = u^n + \Delta t f\left(t^n + \frac{1}{2}\Delta t, u^n + \frac{1}{2}\Delta t f(t^n, u^n)\right). \quad (7)$$

The term $f(t_n, u_n)$ and its variations represent the flux function at its respective point t_n in time.

Fjordholm *et al.* (2008) presented a second-order limited entropy stable fluxes for the system of shallow water equations. Our second-order spatial method is based on a TVD/TVB MUSCL Van Leer (1979) approach. The second-order flux uses a linearly interpolated cell reconstruction with the 'minmod' limiter ($\phi_{\text{mm}}(r)$) defined as

$$\phi_{\text{mm}}(r) = \max[0, \min(1, r)]; \quad \lim_{r \rightarrow \infty} \phi_{\text{mm}}(r) = 1, \quad (8)$$

and the superbee limiter defined as

$$\phi_{\text{sb}}(r) = \max[0, \min(2r, 1), \min(r, 2)]; \quad \lim_{r \rightarrow \infty} \phi_{\text{sb}}(r) = 2, \quad (9)$$

prior to solving f^* at the cell interfaces. The linear (or higher order polynomial) spatial interpolation within each cell only increases the accuracy of velocity inserted into the flux function without altering the form of Equation (4) hence preserving entropy

conservation, stability or consistency. Since a semi-discrete approach is employed, the Runge–Kutta time discretisation (or similar) will still produce an entropy-consistent method.

3. Extending to the Navier–Stokes equations

In vector form, the Navier–Stokes equations can be written as

$$\frac{\partial \mathbf{u}}{\partial t} + \frac{\partial \mathbf{f}}{\partial x} = \frac{\partial \mathbf{u}}{\partial t} + A \frac{\partial \mathbf{u}}{\partial x} = v \frac{\partial \mathbf{f}_v}{\partial x}. \quad (10)$$

Here, v is the viscosity coefficient, \mathbf{u} are the mass, momentum and energy variables while \mathbf{f} , and \mathbf{f}_v their respective inviscid and viscous fluxes.

$$\mathbf{u} = \left(\rho, \rho u, \rho \left(\frac{p(\gamma - 1)}{\rho} + \frac{u^2}{2} \right) \right)^T, \quad (11a)$$

$$\mathbf{f} = \left(\rho u, \rho u^2 + p, \rho u \left(\frac{p(\gamma - 1)}{\rho} + \frac{u^2}{2} + \frac{p}{\rho} \right) \right)^T, \quad (11b)$$

$$\mathbf{f}_v = \left(0, \frac{\partial u}{\partial x}, 0 \right)^T. \quad (11c)$$

Note that this is the Navier–Stokes equations in which the dissipation is due to skin friction; the heat transfer is excluded in this paper to let us focus on the effects of added viscosity towards the inviscid flux. Like the Burgers equation, a similar finite volume discretisation (both first- and second-order time and spatial discretisation methods) is used for the Navier–Stokes equations. The main interest lies in how to discretise the interface fluxes \mathbf{f}^* such that entropy is discretely conserved (equality of Equation (2)), and that the flux function is entropy stable (discretely satisfy Equation (2)) or entropy consistent.

3.1. The scheme of Tadmor–Zhong (2006)

There are a number of entropy-conserved fluxes available in Tadmor (2002) and references therein but the one in Tadmor and Zhong (2006a) (Equations (3.19a) and (3.19b), with the choice of entropy pair as shown in Equation (4.1), and no heat conduction) will be used for comparison purposes. Consider the semi-discrete approximation

$$\frac{d}{dt} \mathbf{u}_v(t) + \frac{1}{\Delta x_v} (\mathbf{f}_{v+\frac{1}{2}}^* - \mathbf{f}_{v-\frac{1}{2}}^*) = \frac{\epsilon}{\Delta x_v} \left(\frac{\mathbf{d}_{v+1} - \mathbf{d}_v}{\Delta x_{v+\frac{1}{2}}} - \frac{\mathbf{d}_v - \mathbf{d}_{v-1}}{\Delta x_{v-\frac{1}{2}}} \right). \quad (12)$$

Here, f^* is an entropy conservative numerical flux

$$f_{v+\frac{1}{2}}^* = \sum_{j=1}^3 \frac{\psi(\mathbf{v}_{v+\frac{1}{2}}^{j+1}) - \psi(\mathbf{v}_{v+\frac{1}{2}}^j)}{\langle \ell_{v+\frac{1}{2}}^j, \Delta \mathbf{v}_{v+\frac{1}{2}} \rangle} \ell_{v+\frac{1}{2}}^j, \quad (13)$$

and \mathbf{v}^{TZV} are the entropy variables used by Tadmor and Zhong (2006a).

$$\mathbf{v}^{\text{TZV}} = U_{\mathbf{u}}(\mathbf{u}) = -(\rho p)^{-\frac{\gamma}{1+\gamma}} \begin{bmatrix} E \\ -m \\ \rho \end{bmatrix}. \quad (14)$$

The entropy pair chosen is

$$(U(\mathbf{u}), F(\mathbf{u})) = \left(\frac{1+\gamma}{1-\gamma} (\rho p)^{\frac{1}{1+\gamma}}, \frac{1+\gamma}{1-\gamma} q(\rho p)^{\frac{1}{1+\gamma}} \right). \quad (15)$$

We leave out heat conduction by setting $\kappa = 0$.

3.2. Entropy stable and entropy-consistent scheme

Let us define another entropy function $U = -\frac{\rho s}{\gamma-1}$ with $s = \ln p - \gamma \ln \rho$ being the physical entropy. Similar to the Burgers' equation, we compute the entropy variables as:

$$\mathbf{v} = \frac{\partial U}{\partial u} = \left(\frac{\gamma-s}{\gamma-1} - \frac{1}{2} \frac{\rho}{p} (u^2), \frac{\rho u}{p}, -\frac{\rho}{p} \right)^T. \quad (16)$$

This choice of entropy variables was selected since it is the only form that can be used in both the Euler and the Navier–Stokes equations (Hughes *et al.* 1986), although there are other choices of entropy variables available as in Tadmor (2002). Entropy stability for the Euler equations Barth (1999) leads to the entropy stable (ES) flux given by those references, which was also used in Ismail and Roe (2009)

$$\mathbf{f}^* = \mathbf{f}_c - \frac{1}{2} \mathbf{R} \mathbf{D} \mathbf{R}^T [\mathbf{v}] = \mathbf{f}_s. \quad (17)$$

In this equation, \mathbf{f}_c is the entropy-conserved flux (Roe unpublished) computed as averaged quantities of its components:

$$\mathbf{f}_c(u_L, u_R) = \begin{bmatrix} \hat{\rho} \hat{u} \\ \hat{\rho} \hat{u}^2 + \hat{p}_1 \\ \hat{\rho} \hat{u} \hat{H} \end{bmatrix}, \quad (18)$$

where the averaged ($\hat{\cdot}$) values are calculated based on equations in Appendix A. The averaged right eigenvectors \hat{R} is

$$\hat{\mathbf{R}} = \begin{bmatrix} 1 & 1 & 1 \\ \hat{u} - \hat{a} & \hat{u} & \hat{u} + \hat{a} \\ \hat{H} - \hat{u} \hat{a} & \frac{1}{2} \hat{u}^2 & \hat{H} + \hat{u} \hat{a} \end{bmatrix}. \quad (19)$$

Next, \hat{D} is a positive dissipation matrix composed of the matrix of absolute eigenvalues and a scaling term

$$\hat{\mathbf{D}} = \hat{\Lambda} \hat{\mathbf{S}} = \begin{bmatrix} |\hat{u} - \hat{a}| & 0 & 0 \\ 0 & |\hat{u}| & 0 \\ 0 & 0 & |\hat{u} + \hat{a}| \end{bmatrix} \begin{bmatrix} \frac{\hat{\rho}}{2\gamma} & 0 & 0 \\ 0 & \frac{(\gamma-1)\hat{\rho}}{\gamma} & 0 \\ 0 & 0 & \frac{\hat{\rho}}{2\gamma} \end{bmatrix}. \quad (20)$$

An entropy-consistent Euler flux (EC2) is written by modifying the dissipative matrix Ismail and Roe (2009)

$$\hat{\mathbf{D}}_{\text{EC2}} = (\hat{\Lambda}_{\text{EC2}} + \alpha_{\text{EC2}} [\Lambda_{u \pm a}]) \hat{\mathbf{S}} \quad (21a)$$

$$\hat{\Lambda}_{\text{EC2}} = \begin{bmatrix} (1+\beta)|\hat{u} - \hat{a}| & 0 & 0 \\ 0 & |\hat{u}| & 0 \\ 0 & 0 & (1+\beta)|\hat{u} + \hat{a}| \end{bmatrix} \quad (21b)$$

$$\alpha_{\text{EC2}} = (\alpha_{\text{max}} - \alpha_{\text{min}}) (\max(0, \text{sign}(dM_{\text{max}} - M))), \quad (21c)$$

where $\beta = 1/6$, $\alpha_{\text{max}} = 2.0$, $\alpha_{\text{min}} = 1/6$, and $dM_{\text{max}} = 0.5$. These additional flux terms ($O[\Delta x^3]$) will be referred to as the entropy production (or third) term \mathbf{f}_p .

The derivation of an entropy-consistency Euler flux was semi-empirically determined in Ismail and Roe (2009), in the sense that the derivation of precise entropy production was based on an analytical formulation of a weak shock with only one intermediate state. For strong shocks with multiple intermediate states, the derivation would require numerical experiments to determine some of the parameters. Note that the viscous fluxes (\mathbf{f}_v) are discretised using a pure central difference as done in the viscous Burgers equation.

The entropy produced for the Euler equations using the ES flux in Ismail and Roe (2009) is

$$\dot{U} = -\frac{1}{2} [\mathbf{v}]^T \mathbf{R} \mathbf{D} \mathbf{R}^T [\mathbf{v}] \leq 0, \quad (22)$$

since it is a product of a positive definite matrix hence generating entropy with the correct sign. In addition, using $\mathbf{D} = \mathbf{D}_{\text{EC2}}$ would ensure the entropy production would be analytically correct for weak shocks and empirically correct for shocks of any strength.

3.3. Incorporating physical viscosity

Similar to the Burgers analysis, including the physical viscosity would then give

$$\begin{aligned} \dot{U} &= -\frac{1}{2} [\mathbf{v}]^T \mathbf{R} \mathbf{D} \mathbf{R}^T [\mathbf{v}] - \frac{v}{(2\Delta x)} [\mathbf{v}]^T (0, [u], 0)^T \\ &= -\frac{1}{2} [\mathbf{v}]^T \mathbf{R} \mathbf{D} \mathbf{R}^T [\mathbf{v}] - \frac{v}{(2\Delta x)} \left[\frac{\rho u}{p} \right] [u], \end{aligned} \quad (23)$$

which implies that the discrete physical viscosity would also generate a decreasing entropy since density and pressure are always positive. Thus, entropy stability is achieved when including the discrete physical viscosity. However, to achieve entropy consistency for the Navier–Stokes would require numerical experiments.

4. Results of Viscous Burgers' equation

Tests were conducted using two shock capturing methods, namely the entropy stable flux with added viscosity (ESV) and the Roe flux with added viscosity (RoeV). Note that when capturing shocks the RoeV flux is identical to the entropy consistent (EC) flux with viscosity. This is not true when capturing expansion fans as was shown in Ismail and Roe (2009). These flux functions were tested with using a wide range of viscosity coefficients ranging from very small ($O(10)^{-7}$) to very large ($O(1)$). However, for brevity, results reported here are for selected values relevant for the respective cases. Tests were run initially using first-order accurate spatial and temporal scheme, followed by the second-order version. The time discretisation method for the second-order version is based on second Runge–Kutta method with 'minmod' limiter for the flux functions.

4.1. Steady shock

The entropy-consistent flux with added viscosity was tested in a steady state shock situation with the following initial conditions:

$$u(x, 0) = \begin{cases} 1, & \text{if } x < 0 \\ -1, & \text{if } x \geq 0. \end{cases} \quad (24)$$

For these tests, 40 computational cells were used with non-reflecting boundary conditions on the left and right sides of the domain. The CFL number was set to 0.1. This low value was chosen due to the constraints that are dictated by both the stability limit of advection-diffusion problem and the nature of explicit semi discrete flux functions which works best using a low CFL number. The flux function based on Burgers' equation works well even when simulated at a CFL value of up to 0.8, but this may not be the case for the Navier–Stokes based scheme. Therefore, to maintain uniformity, the CFL value is kept at 0.1 unless stated otherwise. The fluxes are then compared to the exact solution for Burgers' equation at the corresponding particular value of viscosity being used, as found in Masatsuka (2009):

$$u = \left(1 - \tanh \frac{x}{2v}\right). \quad (25)$$

The first test was done under low viscosity conditions of $v \leq 0.001$. Our results indicate that there are very little differences for these conditions, so only results of $v = 0.001$ are included. As seen in Figure 1(a), the ESV flux exhibits considerable overshoot and undershoot before and after the shock. Although the RoeV (or the ECV) flux provides a closer shock profile to the exact solution, the shock profiles are slightly more diffused than it is supposed to be. This is reflected in

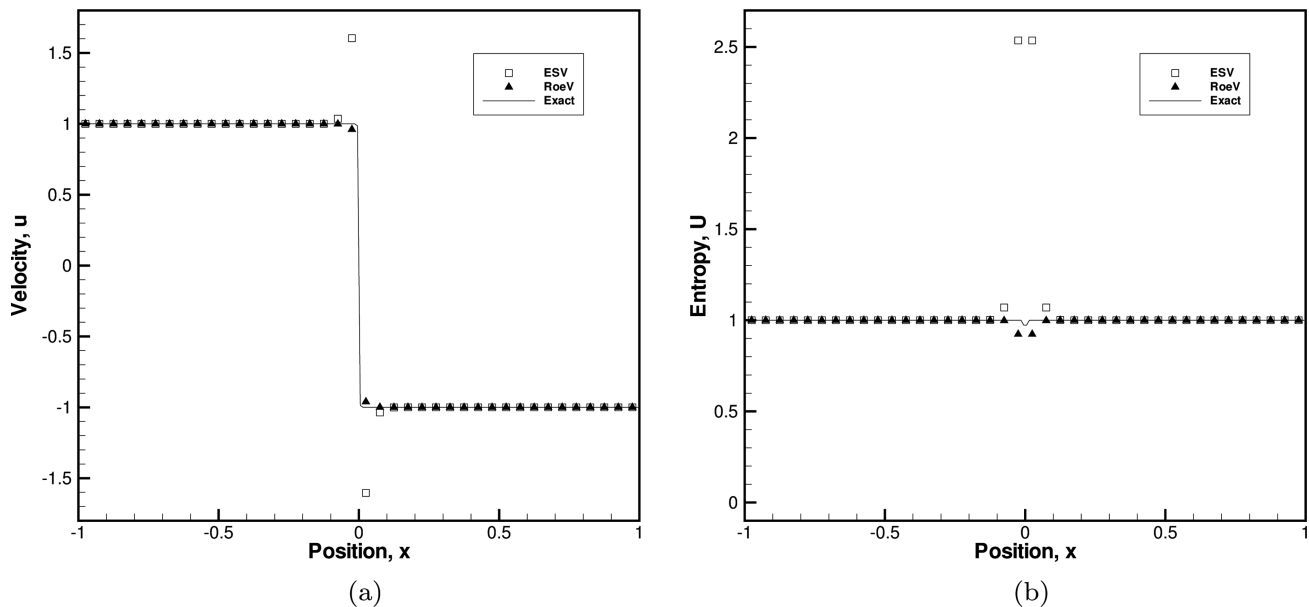


Figure 1. Experiment on Burgers' equation, with viscosity added flux at $v = 0.001$ compared with the corresponding exact solution of (a) velocity and (b) entropy.

Figure 1(b), where the entropy generated for both fluxes are plotted. The RoeV flux produced higher entropy than the exact solution, while the ESV flux underestimates the entropy value by a large margin.

A probable reason for this phenomenon lies in how both the entropy production term and the viscosity term affects the workings of the respective fluxes. For

ESV, the absence of a production term coupled with a low coefficient value for viscosity leads to a result that is severely lacking in entropy production. In contrast, the production term in the RoeV flux is providing more than the necessary amount of entropy to the solution, even with the viscosity being as low as it is. As a result, the ESV flux manifests its entropy inadequacy as

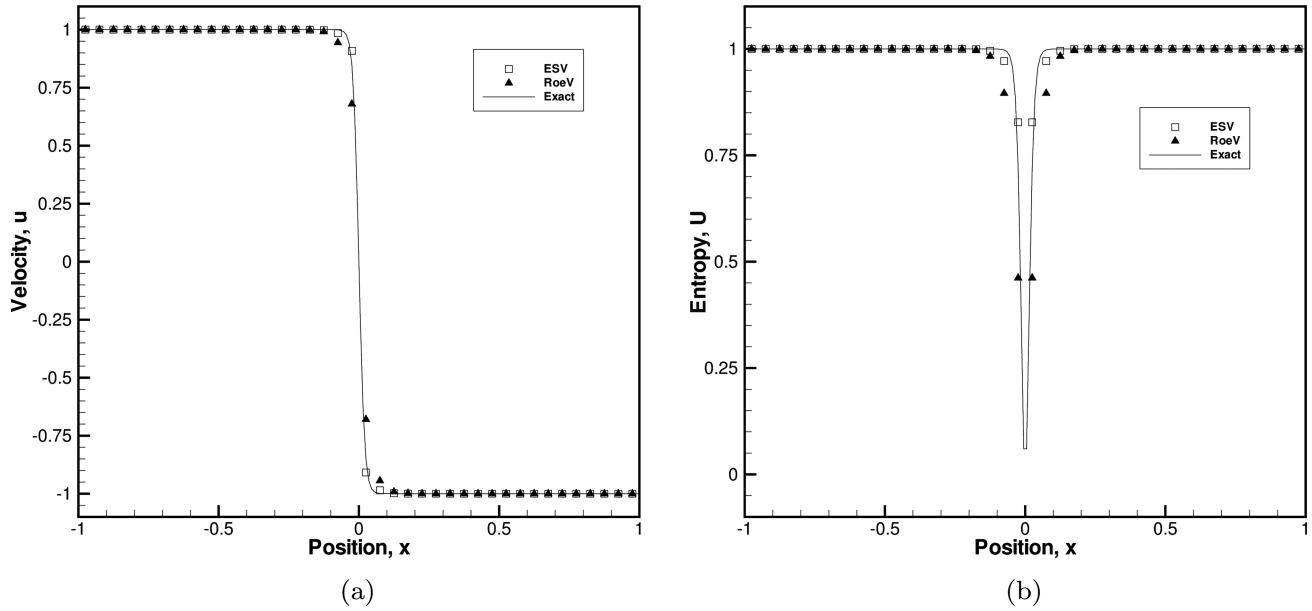


Figure 2. Experiment on Burgers' equation, with viscosity added flux at $\nu = 0.01$ compared with the corresponding exact solution of (a) velocity and (b) entropy.

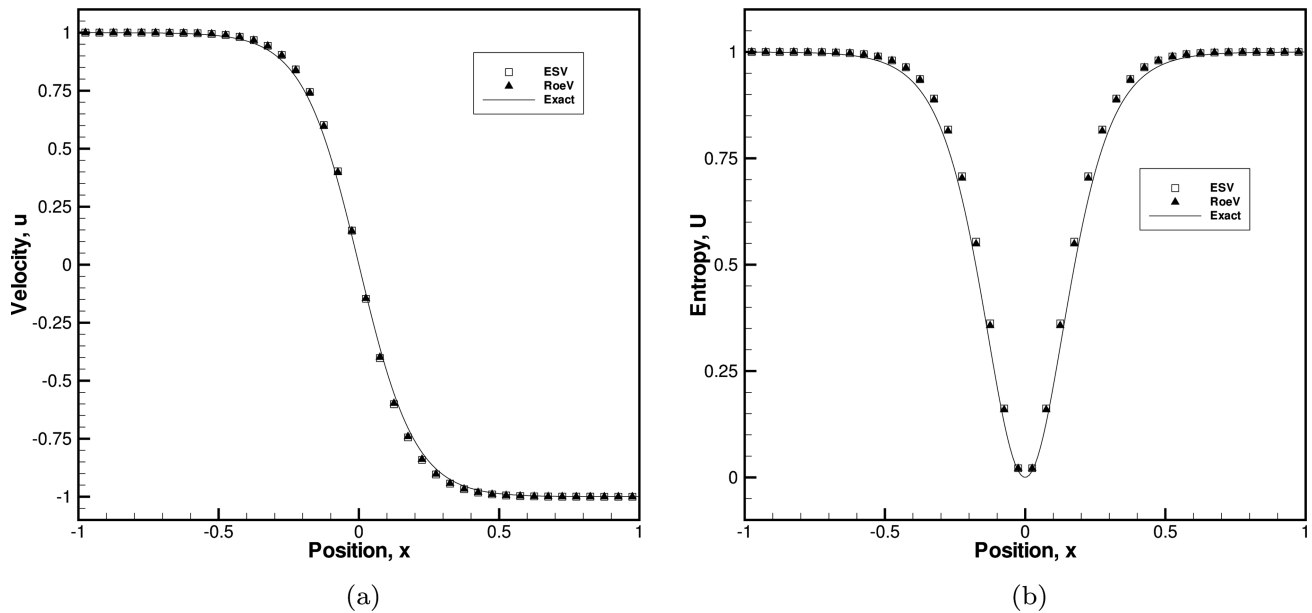


Figure 3. Experiment on Burgers' equation, with viscosity added flux at $\nu = 0.1$ compared with the corresponding exact solution of (a) velocity and (b) entropy.

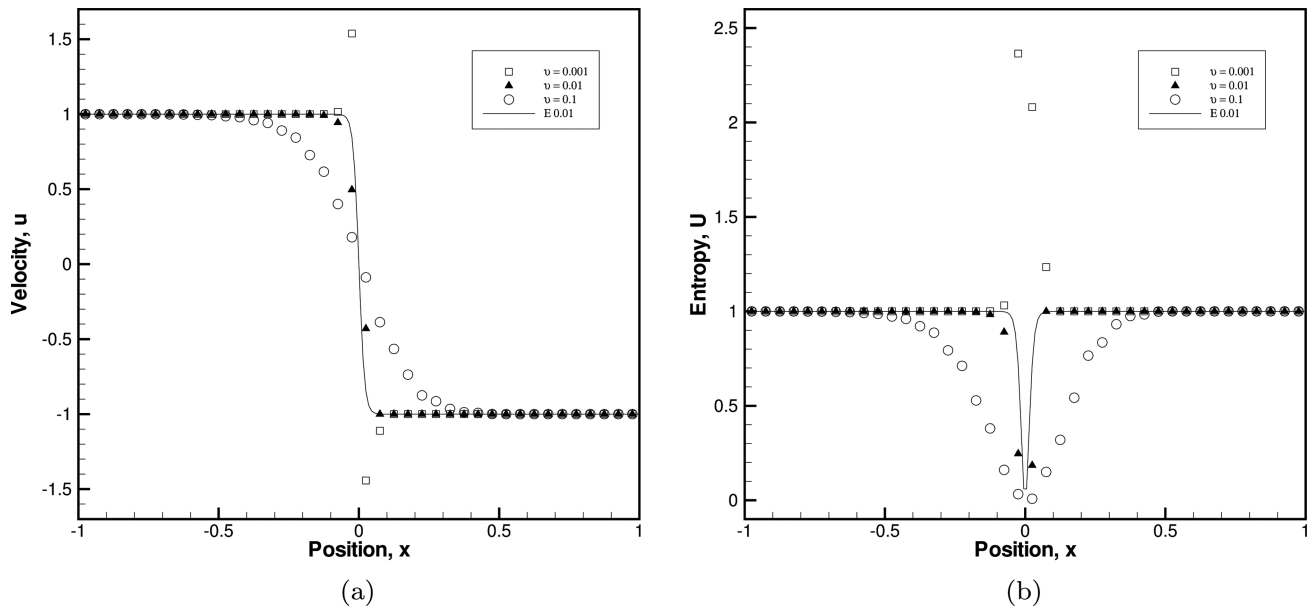


Figure 4. Experiment on Burgers' equation, with viscosity added second-order scheme result for (a) velocity and (b) entropy at various values of ν .

overshoots, while RoeV provides a slightly diffused solution for velocity with the viscosity term proving to be inconsequential for this particular case.

Next, ν is increased to 0.01, with simulation results of velocity shown in Figure 2(a). Compared to the previous condition, the ESV flux no longer exhibits overshoots and is able to match the exact solution reasonably well. Similarly, the RoeV flux also provides a good representation of the shock, but with a slightly more diffused profile than the ESV and exact results. This becomes more apparent in Figure 2(b), looking at the excess amount of entropy produced by the RoeV flux compared to the ESV flux.

For this case, our conjecture is that the physical viscosity coefficient is large enough, enabling the viscosity term in the ESV flux to produce enough entropy without the production term. When the production term is indeed present as is with the RoeV flux, the solution becomes even more diffused, due to more entropy being produced than necessary.

In high viscosity condition ($\nu = 0.1$), the ESV and RoeV fluxes provide almost identical solutions, agreeing reasonably well with the exact solution as seen in Figure 3(a). In Figure 3(b), both flux functions produce almost enough entropy at every point in the domain to match the correct values. For this case, the physical shock profile is less steep, hence it can be viewed as a relatively 'smooth' function compared to previous cases. In this situation, the physical viscosity coefficient ($O(u)^2$) is enough to dominate the solution and relegates the production term ($O(u)^3$) to a negligible role.

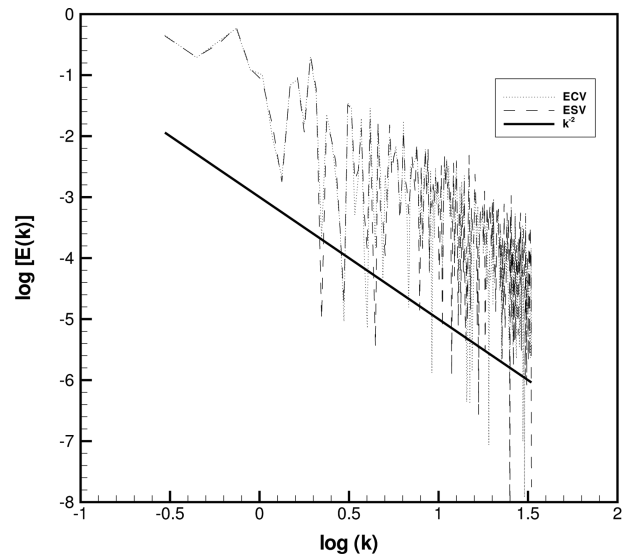


Figure 5. Wavenumber spectra of ESV and ECV fluxes subjected to randomised initial condition.

The results for the second-order ESV flux with 'minmod' limiter are shown in Figure 4. Similar patterns were obtained for all three ν values tested compared to the previous first-order tests. The only difference is that the entropy distribution is no longer symmetric about the shock perhaps due to the nonlinearity of the slope limiting process. Results for the second-order RoeV (or ECV) are also similar to its first-order results and hence not included.

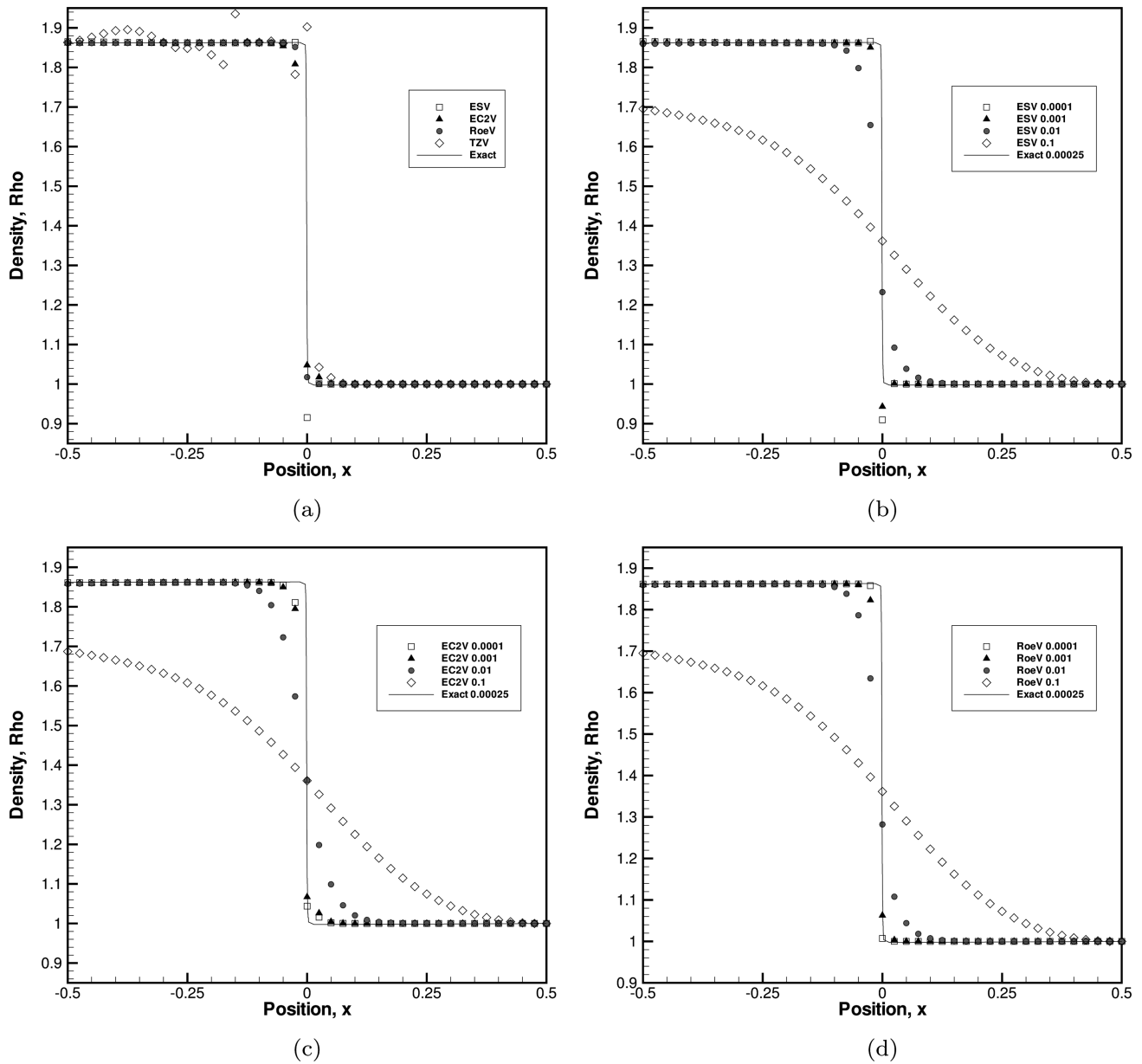


Figure 6. Experiment on Navier–Stokes Equation, with density results from (a) different fluxes, (b) the ESV flux, (c) EC2V flux and (d) RoeV flux compared at various values of ν .

4.2. Burgers problem of turbulence

Figure 5 shows the wavenumber spectra of both the ESV and ECV fluxes. These fluxes were employed in Burgers' problem of turbulence test where the velocity is subjected to random initial condition, with parameters similar to that in Drikakis (2002). The resulting energy spectra from computations of the fluxes are compared to k^{-2} , where k is the wavenumber. The result in Figure 5 is presented without any smoothing functions applied. The ESV and ECV fluxes exhibit similar energy spectra results. Even though the fluxes

produce significantly higher energy compared to the k^{-2} estimate, the trends are similar in that $E(k)$ in general decreases proportionately with the increase in k . Additionally, the slope of a smoothed $E(k)$ function of the fluxes look to be similar to that of k^{-2} . Granted, the spectra of ESV and ECV fluxes are not quite close to the k^{-2} line as the results in Drikakis (2002), but note that these fluxes are only second-order accurate, whilst those in Drikakis (2002) are of higher order of accuracy (third order and above).

5. Results of Navier–Stokes equations

As mentioned in an earlier section, the original entropy-consistent flux function is based on the Euler equations. The inviscid entropy-stable and entropy-consistent fluxes are termed as the ES flux and the EC2 flux, while the extended versions which include the physical viscosity are called ESV and EC2V. A third version of flux that we call RoeV flux, based on the original Roe flux combined with the physical viscosity, was also used. As was the case in the previous section, the CFL value used was maintained at 0.1 for all cases, unless stated otherwise.

5.1. Steady shock

The entropy-consistent flux with added viscosity was tested in a steady state shock situation at Mach 1.5. As in the previous case, a 40 cell setup was used, with non-reflecting boundary conditions on the left and right. The simulation was conducted with flow moving from right to left, to enable data comparison with the exact solution at $\nu = 0.00025$ obtained from Xu (2000). The Rankine-Hugoniot jump initial condition to the left (0) and the right (1) of the shock, respectively,

$$\mathbf{u}_0 = \left[f(M_0) \quad 1 \quad \frac{g(M_0)}{\gamma(\gamma-1)M_0^2} + \frac{1}{2f(M_0)} \right], \quad (26a)$$

$$f(M_0) = \left(\frac{2}{(\gamma+1)M_0^2} + \frac{\gamma-1}{\gamma+1} \right)^{-1}, \quad (26b)$$

$$g(M_0) = \frac{2\gamma M_0^2}{\gamma+1} - \frac{\gamma-1}{\gamma+1}, \quad (26c)$$

$$\mathbf{u}_1 = \left[1 \quad 1 \quad \frac{1}{\gamma(\gamma-1)M_0^2} + \frac{1}{2} \right]. \quad (26d)$$

Results of the Navier–Stokes shock profiles have the same trend compared to the viscous Burgers shock profiles. Figure 6 shows the density results obtained using ESV, EC2V and RoeV fluxes (and for various ν) as compared to the only available exact solution at $\nu = 0.00025$. For low viscosity values ($\nu \leq 0.01$), the ESV flux function produces non-monotone shock profiles unlike the EC2V and RoeV flux functions. The RoeV flux produces a decent result, but the EC2V flux exhibit a bit more diffused shock profile. The ESV flux, however, produces spurious oscillations around the shock which indicates not enough entropy is being generated. These results matches the theoretical expectations since the EC2 flux is designed to produce the correct amount of entropy across shocks compared to the ES flux, ensuring monotonicity in the solution. The RoeV flux generally produces a relatively sharper shock profile than the other fluxes, due to its nature of having minimal numerical dissipation and the small physical viscosity coefficient used in this case.

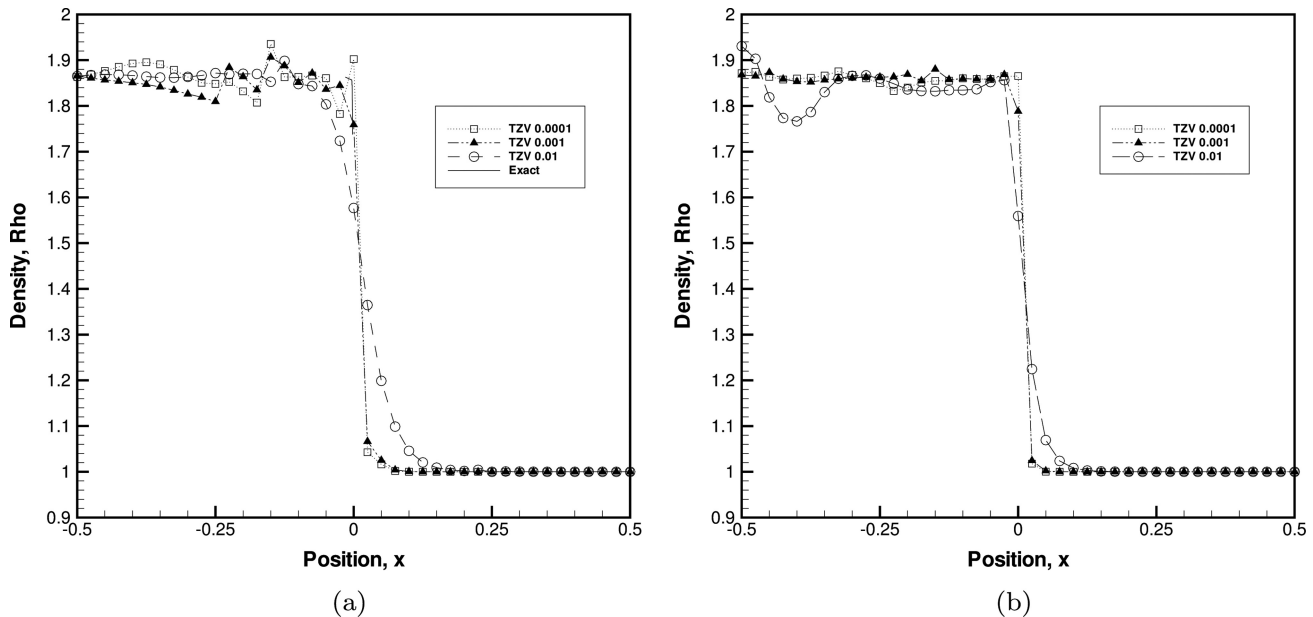


Figure 7. Experiment on Navier–Stokes Equation, with density results from the flux of (a) first-order and (b) second-order Tadmor–Zhong coupled with entropy stability and added viscosity compared at various values of ν .

However, for larger viscosity coefficients ($\nu > 0.01$), all three flux functions produces monotone shock profiles but the RoeV and EC2V results are overly diffusive. For much larger viscosity conditions ($\nu \geq 0.1$), the diffusion is overwhelmingly dominant compared to the inviscid transport mechanism, hence all three flux functions produce almost identical results. Note that the results for velocity and pressure are similar to density hence omitted for brevity.

In Figure 7, the previous case of steady state shock is repeated, but with using the flux of Tadmor–Zhong coupled with (a) first- and (b) second-order entropy

stability term and added viscosity (TZV flux) (Tadmor and Zhong (2006a), Equation (3.19b), with the heat conduction absent as shown in Equation (2.17)). We observe a similar overall pattern to the results using ESV and ECV fluxes as shown in Figure 6, where the change in density before and after the shock occurs more gradually with an increase in physical viscosity. However, in this case, the density after the shock becomes oscillatory with the magnitude of oscillations decreasing with the increase of physical viscosity, but the oscillations increase with the increase of upstream Mach number. In fact, the TZV flux would produce

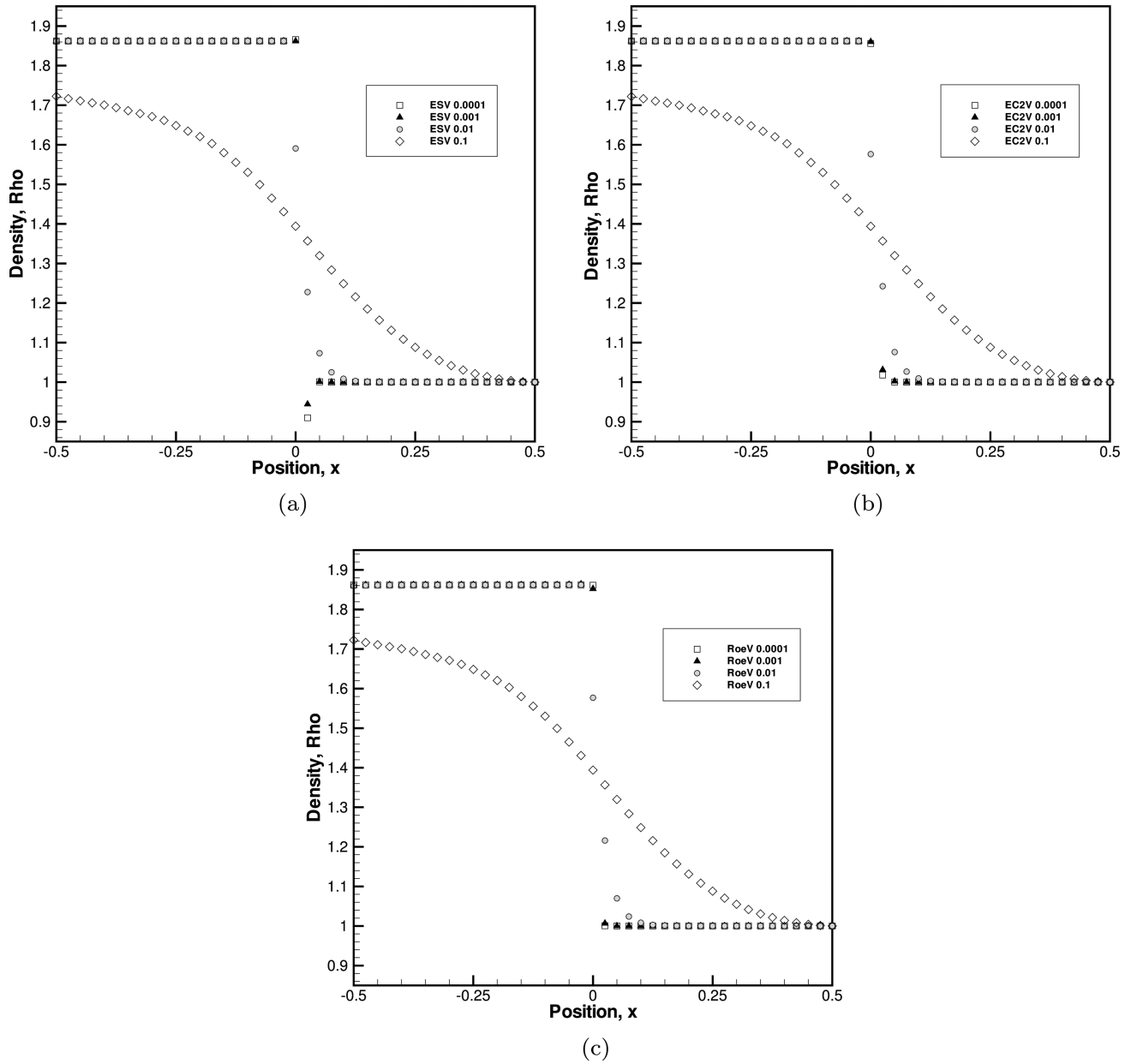


Figure 8. Experiment on second-order Navier–Stokes Equation, with density results from (a) the ESV flux, (b) EC2V flux and (c) RoeV flux compared at various values of ν .

unstable solutions for shocks with very high Mach number flow unlike the ESV or ECV fluxes. For high Mach number flows, the behaviour of the ESV and ECV fluxes are similar to the $Ma = 1.5$ results when physical viscosity is varied.

Figure 8 shows the second-order results as comparison to Figure 6. The method deploys a linear cell interpolation with superbee limiter and second-order Runge–Kutta time discretisation. Overall, the second-order results produce less smeared shock profiles relative to the first-order method. However, first- and second-order methods produce very similar results

when the physical viscosity is very large ($(O)(10^{-1})$ or larger) since the physical viscosity is most dominant.

5.2. Sod’s problem

Next, the fluxes are compared in the case of Sod’s problem where the initial condition for left and right states are

$$[\rho \quad u \quad p]_L = [1.0 \quad 0.0 \quad 1.0 \times 10^5], \quad (27a)$$

$$[\rho \quad u \quad p]_R = [0.125 \quad 0.0 \quad 1.0 \times 10^4]. \quad (27b)$$

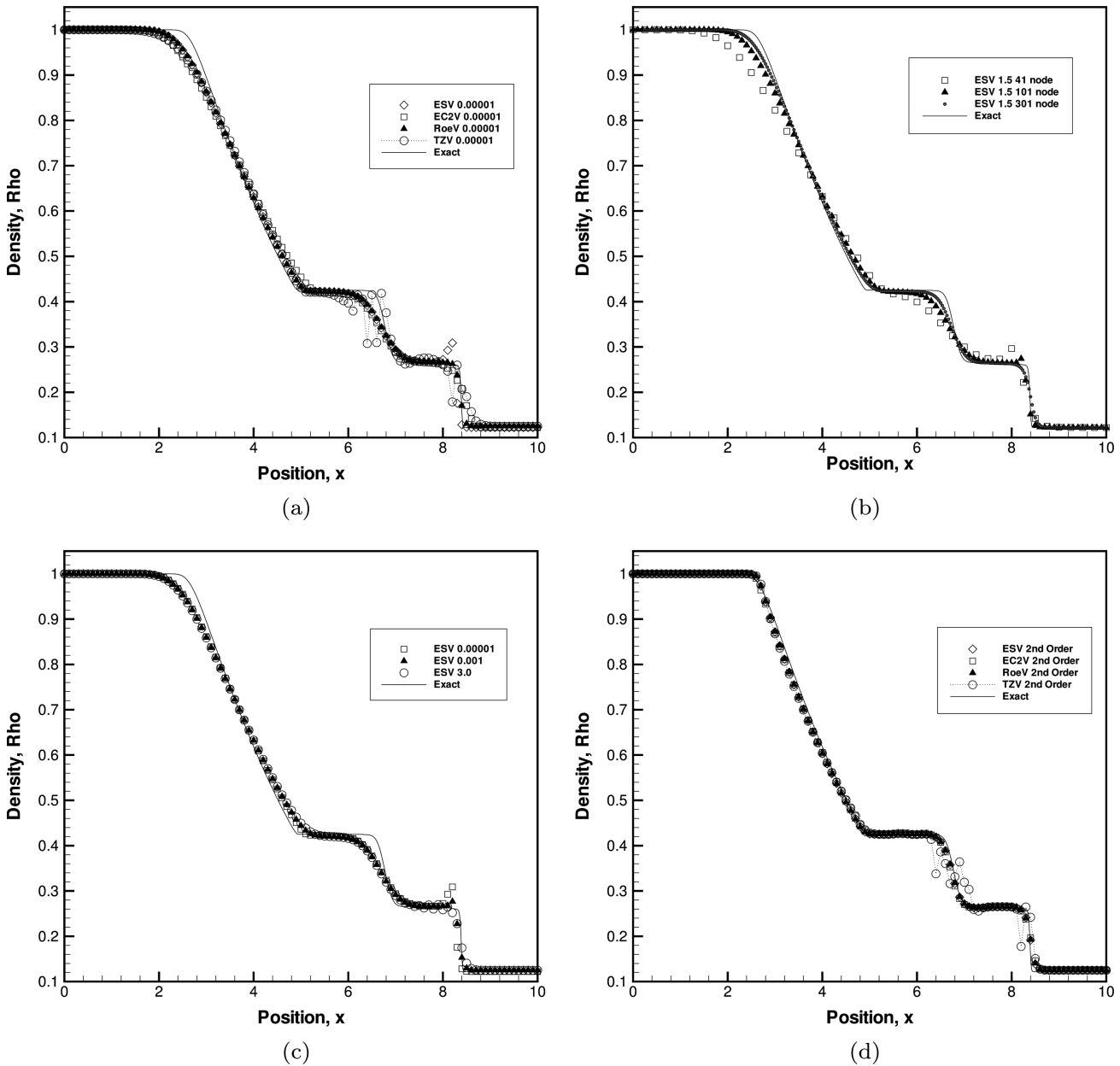


Figure 9. Experiment on Sod’s problem, with viscosity added flux compared with the corresponding exact (inviscid) solution in terms of (a) flux function, (b) cell count, (c) v and (d) second-order flux.

In the first test, with a prescribed cell count of 100 and a CFL number of 0.4, a viscosity value of 0.00001 was chosen to be used for the ESV flux. The result is compared to the EC2V, RoeV and the flux of Tadmor–Zhong coupled with first-order entropy stability and added viscosity (TZV). These solutions are included along with the exact (inviscid) solution in Figure 9(a). We see that the ESV flux with the low viscosity coefficient results in an overshoot at the shock, whilst the TZV flux exhibits oscillatory behaviour at both the contact discontinuity and the shock. Note that for this unsteady case, the EC2V solution is almost identical to RoeV solution, similar to the inviscid results Ismail and Roe (2009). Figure 9(b) shows a similar setup with the same initial conditions as the first. This time, it is the grid size that is varied at 41, 101 and 301 nodes over 10 units of length, with the viscosity coefficient for the ESV flux being kept at 1.5. We observe that the simulation result gets closer to the inviscid solution when the grid size is refined. The same can be said for the TZV method although its results are omitted for brevity. These observations match the expected behaviour of physical viscosity added schemes, as discussed by Tadmor and Zhong (2006a). Figure 9(c) shows how the density profile varies with a change in viscosity. As we have seen before, overshoots are visible at the shock for relatively low values of ν . However, when a high viscosity coefficient was used, the overshoot goes away, resulting in a solution that is close to the RoeV flux. This pattern is true for both the ESV and TZV methods, although only the ESV results are included. Finally, Figure 9(d) shows a similar case to that of Figure 9(a), except that now the fluxes used are of second-order accuracy, aided by the minmod limiter. The result of the second-order case follows the pattern of its first-order counterpart; it is particularly clear that the oscillations of the TZV flux near contact discontinuity and the shock becomes more accentuated as compared to the first-order case.

6. Conclusion

There have been some recent studies in applying the physical viscosity to replace the numerical viscosity in solving the problems in conservation laws (Tadmor and Zhong 2006a, Fjordholm *et al.* 2008). The results obtained therein showed that coupling some form of entropy conserving flux (no numerical diffusion) and physical diffusion produced oscillatory solutions around the shock for relatively coarse grids and the magnitude of these oscillations start to decrease as the grids were refined and eventually disappear for extremely fine grids (Tadmor and Zhong 2006a). This is because as the grids are refined, the Navier–Stokes true shock structure would be revealed perhaps

reducing the dependence on artificial diffusion (Ismail and Roe 2009). Unfortunately, these extremely fine grids must be finer than the shock thickness which is not practical for most CFD calculations. There are also studies in laminar and turbulent flows which have shown that the numerical viscosity can be totally removed while maintaining a relatively good accuracy (Thornber *et al.* 2008, Drikakis *et al.* 2009), but these works only focussed mostly on smooth flows and to certain extent, very weak shocks.

Our results show that to predict a satisfactory shock of any strength on a reasonably practical grid size would require some form of numerical dissipation in addition to the physical viscous dissipation. If only the physical viscosity is used, the shock solutions will be oscillatory for extremely weak shocks even for first-order methods and unstable for any shock in general. When solving the Navier–Stokes, entropy consistency can be achieved by using the entropy-conserved flux coupled with the physical viscosity discretisation and at least including the entropy-stable (second) term for high viscosity conditions ($\nu \geq 0.01$). This does not imply that the entropy production (EP) in Equation (4d) for entropy consistency proposed in Ismail and Roe (2009) based purely on Euler formulations to be incorrect. However, results herein merely demonstrate that the EP term is not always needed to achieve entropy consistency. In fact, our results indicate that both second and third artificial viscosity terms are required for low viscosity (high Reynolds number) flow which is consistent to the Euler results.

Our proposed entropy-consistent Navier–Stokes flux has the following form:

$$\mathbf{f}^* = \mathbf{f}_s - \max(0, \text{sgn}(\nu - \nu_{\text{crit}})\mathbf{f}_p) - \mathbf{f}_v, \quad (28)$$

where sgn and ν_{crit} are the sign function and the critical viscosity values empirically determined to be 0.01. Note that this is just a preliminary study in which the Navier–Stokes equations are without heat transfer although we hope to address this in the near future. Overall, the approach we are taking in this paper is limited for laminar flow where the physical viscosity is constant. Developing a similar flux function for computational turbulence, where the eddy viscosity varies locally perhaps will not be straightforward and this will be left as one of the avenues for future work.

Acknowledgements

This research was supported in part by Universiti Sains Malaysia Research University grant (No:1001/PAERO/814152), Universiti Tun Hussein Onn Malaysia and scholarship from the Malaysian Ministry of Higher Education.

References

- Barth, T.J., 1999. Numerical methods for gasdynamic systems on unstructured meshes. In: M.O.D. Kroner and C. Rhode, eds. *An introduction to recent developments in theory and numerics for conservation laws*. Lecture Notes in Computational Science and Engineering 5. Berlin: Springer-Verlag, 195–285.
- Drikakis, D., 2002. Embedded turbulence model in numerical methods for hyperbolic conservation laws. *International Journal for Numerical Methods in Fluids*, 39, 763–781.
- Drikakis, D., *et al.*, 2009. Large eddy simulation using high resolution and high-order methods. *Philosophical Transactions of the Royal Society A*, 367, 2985–2997.
- Fjordholm, U.S., Mishra, S., and Tadmor, E., 2008. Energy preserving and energy stable schemes for the shallow water equations. In: *Foundations of computational mathematics, Hong Kong 2008*. London Mathematical Society Lecture Note Series 363. Boston, MA: Cambridge University Press, 93–139.
- Harten, A. and Hyman, J.M., 1983. Self-adjusting grid method for one-dimensional hyperbolic conservation laws. *Journal of Computational Physics*, 50, 235–269.
- Hughes, T., Franca, L., and Mallet, M., 1986. A new finite element formulation for compressible fluid dynamics: I. Symmetric forms of the compressible Euler and Navier Stokes equations and the second law of thermodynamics. *Computer Methods in Applied Mechanics and Engineering*, 54, 223–234.
- Ismail, F., 2006. *Toward a reliable prediction of shocks in hypersonic flow: resolving carbuncles with entropy and vorticity control*. Thesis (PhD). The University of Michigan, USA.
- Ismail, F. and Roe, P., 2009. Affordable entropy consistent Euler flux functions II: Entropy production at shocks. *Journal of Computational Physics*, 228, 5410–5436.
- Kitamura, K., Roe, P., and Ismail, F., 2009. Evaluation of Euler fluxes for hypersonic flow computations. *AIAA Journal*, 47, 44–53.
- Lefloch, P., Mercier, J., and Rohde, C., 2002. Full discrete entropy conservative schemes of arbitrary order. *SIAM Journal on Numerical Analysis*, 40, 1968–1992.
- Masatsuka, K., 2009. *I do like CFD, Vol. 1: governing equations and exact solutions*. Self-published
- Roe, P.L., unpublished. *Affordable, entropy-consistent, Euler flux functions I. Analytical results*. Unpublished.
- Roe, P., 1981. Approximate Riemann solvers, parameter vectors and difference schemes. *Journal of Computational Physics*, 43, 357–372.
- Tadmor, E., 1987. The numerical viscosity of entropy stable schemes for systems of conservation laws. *Mathematics of Computation*, 49, 91–103.
- Tadmor, E., 2002. Entropy stability theory for difference approximations of nonlinear conservation laws and related time dependent problems. *Acta Numerica*, 12, 451–512.
- Tadmor, E., 2004. Burgers' equation with vanishing hyperviscosity. *Communications in Mathematical Sciences*, 2, 317–324.
- Tadmor, E. and Zhong, W., 2006a. Entropy stable approximations of Navier–Stokes equations with no artificial numerical viscosity. *Journal of Hyperbolic Differential Equations*, 3, 529–559.
- Tadmor, E. and Zhong, W., 2006b. Novel entropy stable schemes for 1D and 2D fluid equations. In: S. Benzoni-Gavage and D. Serre, eds. *“Hyperbolic Problems: Theory, Numerics, Applications”*, *Proceedings of the 11th International Conference*, July 2006, Lyon. Berlin: Springer, 1111–1120.
- Thornber, B., *et al.*, 2008. On entropy generation and dissipation of kinetic energy in high-resolution shock-capturing schemes. *Journal of Computational Physics*, 227, 4853–4872.
- Van Leer, B., 1979. Toward the ultimate conservative difference scheme V. A second order sequel to Godunov's method. *Journal of Computational Physics*, 32, 101–136.
- Xu, K., 2000. Gas kinetic schemes for fluid simulations. In: N. Satofuka, ed. *1st International Conference on Computational Fluid Dynamics*, Kyoto, Japan, 10–14 July 2000. Germany: Springer, 14–23.

Appendix A. Entropy conserving flux

The entropy conserving flux from Equation (18) satisfies

$$\mathbf{v}^T \mathbf{f}_c = [\rho \mathbf{u}], \quad (\text{A1})$$

and is calculated based on averaged quantities of

$$\mathbf{f}_c(\mathbf{u}_L, \mathbf{u}_R) = \begin{bmatrix} \hat{\rho} \hat{u} \\ \hat{\rho} \hat{u}^2 + \hat{p}_1 \\ \hat{\rho} \hat{u} \hat{H} \end{bmatrix}. \quad (\text{A2})$$

To determine the averaged quantities, we firstly define $z_1 = \sqrt{\frac{\rho}{p}}$, $z_2 = \sqrt{\frac{\rho}{p}} u$, $z_3 = \sqrt{\rho p}$. The averaged quantities are composed from functions of arithmetic mean $\bar{a} = \frac{a_L + a_R}{2}$ and logarithmic mean as defined in Appendix B. Based on equation A1, the quantities used in the flux are as follows

$$\hat{u} = \frac{\bar{z}_2}{\bar{z}_1}, \quad \hat{\rho} = \bar{z}_1 z_3^{\ln}, \quad \hat{p}_1 = \frac{\bar{z}_3}{\bar{z}_1}, \quad \hat{p}_2 = \frac{\gamma + 1}{2\gamma} \frac{z_3^{\ln}}{z_1^{\ln}} + \frac{\gamma - 1}{2\gamma} \frac{\bar{z}_3}{\bar{z}_1}, \quad (\text{A3})$$

$$\hat{a} = \left(\frac{\gamma \hat{p}_2}{\hat{\rho}} \right)^{\frac{1}{\gamma}}, \quad \hat{H} = \frac{\hat{a}^2}{\gamma - 1} + \frac{\hat{u}^2}{2}. \quad (\text{A4})$$

Appendix B. Logarithmic mean

Let $\zeta = \frac{a_L}{a_R}$. Define $a^{\ln}(\mathbf{L}, \mathbf{R}) = \frac{a_L + a_R}{\ln(\zeta)} \frac{\zeta - 1}{\zeta + 1}$ where

$$\ln(\zeta) = 2 \left(\frac{1 - \zeta}{1 + \zeta} + \frac{1(1 - \zeta)^3}{3(1 + \zeta)^3} + \frac{1(1 - \zeta)^5}{5(1 + \zeta)^5} + \frac{1(1 - \zeta)^7}{7(1 + \zeta)^7} + O(\zeta^9) \right).$$

To calculate the logarithmic mean we use the following subroutine:

Algorithm B.1

- (1) Set the following: $\zeta = \frac{a_L}{a_R}$, $f = \frac{\zeta - 1}{\zeta + 1}$, $u = f * f$
- (2) If ($u < \epsilon$)
- (3) $F = 1.0 + u/3.0 + u * u/5.0 + u * u * u/7.0$
- (4) Else

$$F = \ln(\zeta)/2.0/(f)$$

thus

$$a^{\ln}(\mathbf{L}, \mathbf{R}) = \frac{a_L + a_R}{2F}, \quad \epsilon = 10^{-2}.$$